Palaeogeography, Palaeoclimatology, Palaeoecology 622 (2023) 111577

Contents lists available at ScienceDirect

Palaeogeography, Palaeoclimatology, Palaeoecology

journal homepage: www.elsevier.com/locate/palaeo

A re-evaluation of Holocene relative sea-level change along the Fujian coast, southeastern China

Fengling Yu [a,b,*], Nannan Li [a,*], Ganghua Tian [a], Zhaoquan Huang [a], Haixian Xiong [c,d], Tanghua Li [e], Shengtao Liu [a], Yuze Liu [a]

[a] College of Ocean and Earth Sciences, State Key Laboratory of Marine Environmental Science, Xiamen University, Xiamen, China
[b] Fujian Provincial Key Laboratory for Coastal Ecology and Environmental Studies, Xiamen University, Xiamen, China
[c] School of Marine Sciences, Sun Yat-sen University, Zhuhai, China
[d] Southern Marine Science and Engineering Guangdong Laboratory (Zhuhai), Zhuhai, China
[e] Earth Observatory of Singapore, Nanyang Technological University, Singapore

ARTICLE INFO

Editor: M Elliot

Keywords:
Sea-level change
GIA
Fujian
Far-field
Tectonic effects
Holocene

ABSTRACT

The southeastern China coast is a region of special interest in the study of past and present relative sea-level change, given its distal location from giant ice sheets (far-field regions). During the past decades, a large number of biological, geological, and archaeological sea-level indicators have been retrieved from the Fujian coastal region which allows for recalibration and recalculation of sea-level index points (SLIPs). This study constructs a database of Holocene relative sea-level (RSL) observations for the Fujian coast, southeastern China. The database contains 59 quality-controlled SLIPs which show that RSL for the Fujian coast did not exceed present (0 m) during the Holocene, except potentially during 7.5–5.5 cal. kyr BP and 1.8–0.7 cal. kyr BP. Rates of RSL change were highest during the early Holocene and have decreased over time, due to the diminishing response of the Earth's mantle to glacial isostatic adjustment (GIA) and reduction of meltwater input. A series of sea-level oscillations were recorded in our SLIPs-based reconstructions which might correspond to global climate warming or cooling events. We assessed the spatial variability of RSL histories and compared these with the ICE-6G_C and ANU-ICE GIA model predictions. Substantial misfits between GIA predictions and regional RSL reconstructions were recognized: (1) the deceleration of the early-Holocene sea-level rise ended about one millennia earlier in the ICE-6G_C model than in the SLIPs-based reconstructions; (2) GIA model predictions show a mid-Holocene sea-level highstand of 1–3 m which is absent from our SLIPs-based reconstructions; and (3) all GIA model predicted a gradual RSL fall to 0 m since the middle Holocene, while our reconstruction displays significant RSL oscillations. It is presently unknown whether these misfits are caused by uncertainties in regional tectonic movement estimation or parameters used in the GIA models. Future applications of spatiotemporal statistical techniques are required to better quantify the gradient of the isostatic contribution and to provide improved context for the assessment of the ongoing acceleration of sea-level rise.

1. Introduction

Human-induced global warming has led to accelerated sea-level rise, which is threatening coastal areas globally and becomes one of the major concerns of our society (Fox-Kemper et al., 2021). Numerical simulations suggest that, with medium confidence, the global mean sea level could rise by 0.40–0.81 m by the end of this century under different Shared Socioeconomic Pathway (SSP) emission scenarios (Fox-Kemper et al., 2021). Observed twentieth-century global mean sea-level change is attributed to anthropogenic greenhouse gas emission. However, modern sea-level monitoring record is comparatively short relative to earth's history, so knowledge of how the global or regional sea-level have responded to natural climate change and anthropogenic forcing during the pre-industrial time is still indispensable (Slangen et al., 2016). Geological records of past sea-level change can significantly extend the sea-level history far beyond recent and therefore constitute an important supplement to the current sea-level database. The long-term sea-level reconstructions will improve the understanding of the

* Corresponding authors at: College of Ocean and Earth Sciences, State Key Laboratory of Marine Environmental Science, Xiamen University, China.
E-mail addresses: fengling.yu@xmu.edu.cn (F. Yu), linannan@xmu.edu.cn (N. Li).

https://doi.org/10.1016/j.palaeo.2023.111577
Received 27 January 2023; Received in revised form 12 April 2023; Accepted 17 April 2023
Available online 20 April 2023

causes and patterns of global or regional sea-level change at different time scales and could ultimately contribute to a better assessment of the potential impacts of sea-level oscillations on coastal lands and ecosystems (Milne et al., 2009; Gehrels and Shennan, 2015; Costas et al., 2016; Wang et al., 2023). Moreover, geological archive-based long-term and high-precision reconstruction of the sea-level change is essential for understanding models of Earth's rheology and glacial-isostatic adjustment (GIA), which will improve the reliability of the predictions of future sea-level change (e.g., Lambeck et al., 2002; Peltier, 2004; Engelhart and Horton, 2012; Peltier et al., 2022).

Today's understanding of sea-level change developed through a combination of process-based physical modelling and long-term observational data (Mauz et al., 2015). The climate transition from the last glaciation maximum (LGM) to the Holocene represents one of the most interesting periods, during which the global mean sea level increased from ~120 m below present to its modern level (Clark and Mix, 2002; Lambeck et al., 2002, 2014; Peltier et al., 2022). This transition period provided us with a unique opportunity to assess the potential impacts of ongoing sea-level rising on coastal areas under current global warming circumstances. However, previous studies have found that even within a specific region, although the relative sea-level (RSL) curves agree with each other in general, they can be different in detail due to differences in GIA, tectonics, and local processes (Milne et al., 2009; Kopp et al., 2015; Khan et al., 2015). For instance, along the Atlantic coast of Europe, the reconstructed sea level displayed spatial variability which can be attributed to the deglaciation of the British-Irish and Fennoscandian Ice sheets (Carlson and Clark, 2012; Cuzzone et al., 2016; García-Artola et al., 2018).

In the far-field of the former ice sheets, the RSL signal varies due to the variable response of the earth to ocean loading, and the RSL signal was dominated by the rate and magnitude of meltwater input into the oceans (e.g., Mauz et al., 2015; Khan et al., 2015; Bradley et al., 2016). As eustatic contributions to RSL change usually exceeded glacio-isostatic contributions in far-field regions (e.g., Mauz et al., 2015; Khan et al., 2015), improved knowledge about far-field sea-level change can help better constrain the evolution of high-latitude ice sheets which is a fundamental parameter in climate models (Bassett et al., 2005; Stanford et al., 2011). However, while the general variation trend of the far-field sea-level signal is known (e.g., Bassett et al., 2005; Khan et al., 2015), the effects and the mechanisms on a regional scale is still poorly constrained due to insufficient observations over wider areas in the far-field (Bassett et al., 2005; Stanford et al., 2011), particularly in East Asia (Khan et al., 2015). Investigations of Holocene RSL in the far-field region of Asia are mostly concentrated in Southeast Asia (e.g., Horton et al., 2005; Bird et al., 2010; Chua et al., 2021), although studies have expanded in recent years to include South Korea, the Philippines, China, the Malay-Thai peninsula, and Japan (cf. Khan et al., 2015 and reference therein). In most far-field RSL records, Holocene RSL curves are characterized by a mid-Holocene highstand which varies in magnitude and timing (e.g., Horton et al., 2005; Woodroffe and Horton, 2005; Bird et al., 2010; Khan et al., 2015; Chua et al., 2021).

The eastern China coast represents one of the most complicated far-field regions where the sea-level history is significantly influenced by tectonic movements and local processes (e.g., Zheng et al., 2013). In addition to meltwater inputs, RSL reconstructions for the eastern China coast may also be influenced by active subduction zone tectonics from the collision of the Eurasian, Indian, Philippine, and Pacific plates or sediment loading from large river deltas (Zong, 2004). Zong (2004) collected and calibrated 235 sea-level index points (SLIPs) and reconstructed sea-level histories for six sub-divided regions along the southeast coast of China. The reconstructed sea-level histories displayed obvious spatial variabilities and the timing and height of the mid-Holocene sea-level highstand varied significantly among different coastal regions of southeastern China (Zong, 2004). In particular, RSL reconstructions for Fujian and east Guangdong coasts indicate a significant mid-Holocene sea-level highstand, whereas the height of the mid-Holocene highstand of other regions is much lower (cf. Zong, 2004). Zong (2004) suggested that local processes, such as tectonic movements and sedimentary processes, may have modified the middle- to late-Holocene sea-level history of the Fujian and eastern Guangdong coasts. Due to the lack of proper estimation of tectonic effects and local processes, Zong (2004) didn't present the corrected Holocene RSL reconstructions for those two regions. In recent years, sea-level reconstructions for the eastern China coasts have significantly increased and have expanded to include RSL reconstructions from the Bohai Bay (e.g., Wang et al., 2015, 2020; Li et al., 2021), the Yangtze River Delta (Wang et al., 2012, 2013; Liu et al., 2015, 2018; Xiong et al., 2020), and the Pearl River Delta (Xiong et al., 2018). However, compared to the above areas, Holocene RSL reconstructions for the Fujian coast are still sparse.

Along the Fujian coast, evidence of Holocene RSL change is preserved in abundant geomorphological and sedimentary archives. As RSL can be reconstructed from index points that mark sea-level positions at a given place and time, there are pioneering studies that have used pre-existing sea-level data to reconstruct the sea-level history along the Fujian coast (Fig. 1): RSL reconstructions along the Fujian coast extend nearly twenty thousand years into the past and differ significantly across the region (Guo, 1979; Lan et al., 1986; Yang and Zheng, 1990; Zeng, 1991; Wang et al., 1994; Li et al., 2016; Wang et al., 2022). However, existing analyses only use a small subset of Fujian RSL data, many of which were produced in the 1980's or earlier (e.g., Guo, 1979; Lan et al., 1986, and references therein) and have yet to be aggregated into a quality-controlled, standardized database. Small datasets and a lack of data aggregation and standardization make it hard to disentangle and understand the different processes that drive RSL change along the Fujian coast.

Here, we select and compile a quality-controlled RSL database spanning the Fujian coast, in southeastern China. The comprehensive database consists of SLIPs from various geomorphological and sediment records. To compile the data and estimate their uncertainties, we employ standard procedures agreed upon by the sea-level community (e.g., Hijma et al., 2015; Khan et al., 2019) that include defining each indicator's indicative meaning to sea-level, calibrating ages to current standards, and assessing sources of temporal and vertical uncertainties. We employ a Gaussian process (GP) regression model to reconstruct the Holocene RSL along the Fujian coast. Moreover, to examine the GIA

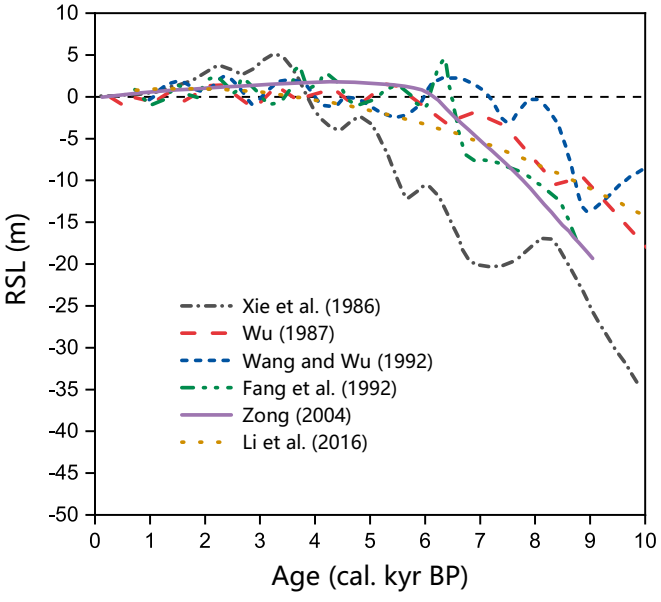

Fig. 1. Published SLIPs-based sea-level reconstructions along the Fujian coast (cf. Xie et al., 1986; Wu, 1987; Wang and Wu, 1992; Fang et al., 1992; Zong, 2004; Li et al., 2016).

processes across this region, the 3D Earth model HetM-LHL140 coupled with ICE-4G, ICE-6G_C, and ANU-ICE models were used to produce the predicted RSLs for the Fujian coast. Our reconstruction yield insights into the deglacial sea-level dynamics of the region. We conclude by discussing the spatio-temporal variabilities of Holocene RSL that possibly contributed to the explanation of tectonic and local processes that influence the sea-level change patterns observed in these data.

2. Regional settings of the study area

Fujian is an administrative province located on the southeastern coast of China, facing the Taiwan Strait (Fig. 2a and b). From a tectonic perspective, Fujian belongs to the Southern China Fold System surrounding the Pacific Ocean and is characterized by a series of magma eruptions and fault activities during the Mesozoic and the Cenozoic (Li, 1993; Chen et al., 2002). Fault structures are very common in this area and are a dominant factor that controls magmatic activity and coastal landform formation and development (Fig. 2c): The geological structure framework for this region is controlled by a series of NE-trending and NW-trending faults. The NE-trending faults include deep faults, such as the Zhenghe-Dabu Fault, Changle-Dongshan Fault, and the Coastal Fault Zone. Whereas the NW-trending faults include the Shanghang-Yunxiao Fault, Shunchang-Minqing Fault, Minjiang River Fault, and Jiulong River Fault, etc. (Li, 1988; Li, 1993; Chen et al., 2002).

The climate in Fujian province is deeply influenced by the East Asian monsoon system and is characterized by abundant precipitation, with hot summers but mild winters (subtropical maritime monsoon climate). Due to the special location and subtropical climate, the Fujian coast represents one of the most frequent areas of typhoon storm events in China (e.g., Shi et al., 2015). Along the Fujian coast, the Minjiang Estuary (in the north) and its adjacent coastal areas are the most frequently-influenced by severe typhoon storms (e.g., Shi et al., 2015). The tidal range (difference between the high-water level and lower-water level) for the northern and middle Fujian coast is higher than that for the southern Fujian coast. The average tidal range of Sansha Bay at the northern Fujian coast, is reported to be higher than 5 m, representing the very high tidal range reported along China's coast (China Gulf Chronicles Compilation Committee (CGCC), 1993).

3. Materials and methods

3.1. Sea-level index points (SLIPs) collection and selection

Previous studies have reported abundant evidence of past sea-level change that is preserved in coastal geological archives (e.g., Guo, 1979; Lan et al., 1986; Yang and Zheng, 1990; Zeng, 1991; Wang et al., 1994; Li et al., 2016), however, not all those previously-reported SLIPs can be used for reliable sea-level reconstruction, especially when considering the reliability and uncertainties between different sea-level indicators or dating methods. We, therefore, conducted a screening of the raw SLIPs dataset, resulting in 59 SLIPs points for the Fujian coastal area used in this reconstruction (Table 1). Those SLIPs were selected mainly based on the following selection criteria: (1) each SLIP should have an unambiguous indicative meaning of past sea-level change

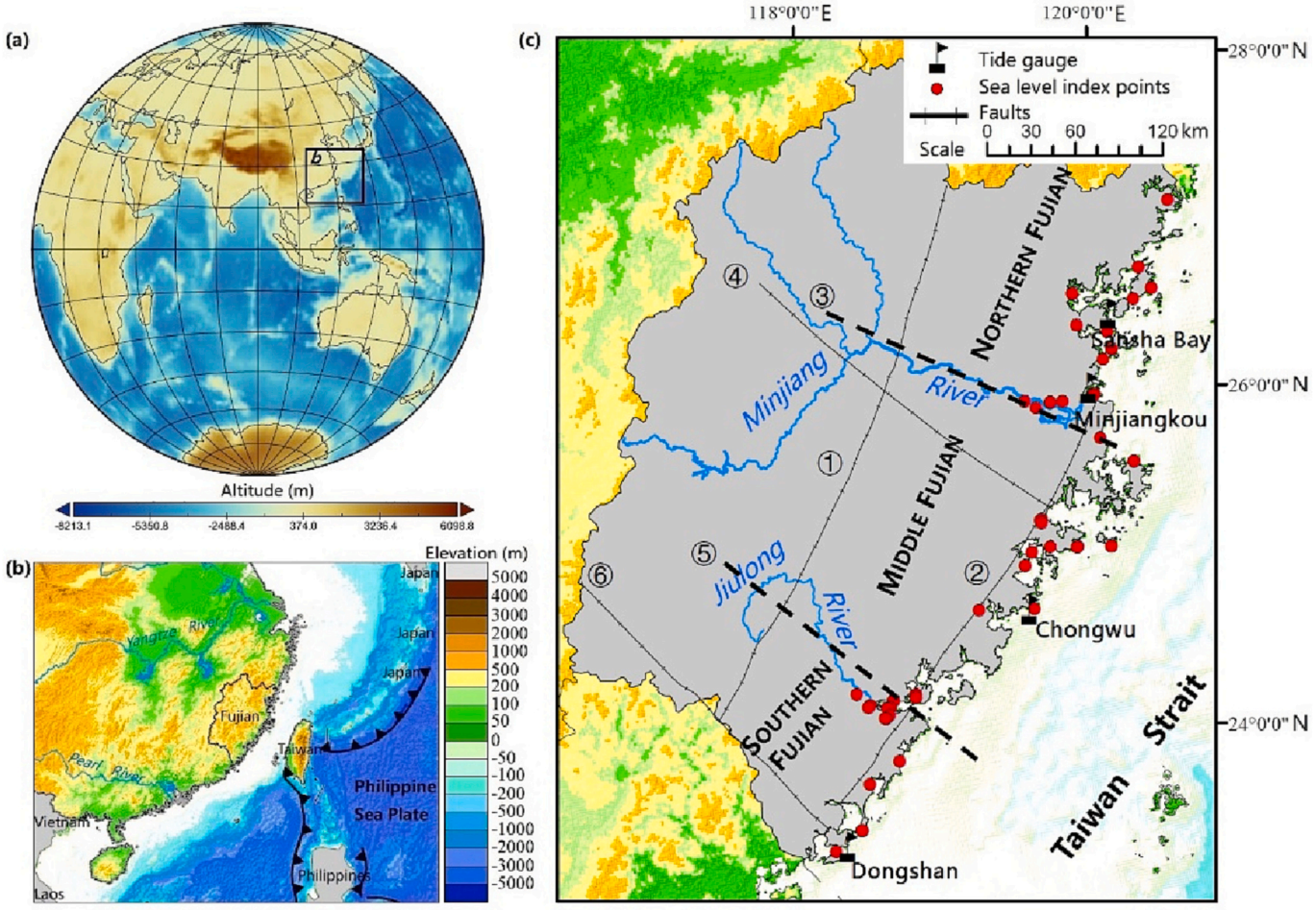

Fig. 2. The location (a), geographical settings of the study region (b), and spatial distribution of the sea level index points dataset used in this study (c). ① the Zhenghe-Dabu Fault; ② the Changle-Dongshan Fault; ③ the Minjiang River Fault; ④the Shunchang-Minqing Fault; ⑤ the Jiulong River Fault; ⑥ the Shanghang-Yunxiao Fault.

Table 1
Recalibrated Holocene SLIPs database for the Fujian coast.

Subregion	Sediment type	Latitude	Longitude	C14 date (yr BP)	**Cal. age (cal. yr BP)**	Calibrated age (2σ, cal. yr BP)	*Altitude (m YSD)*	*Indicative meaning (m)*	*Sediment compaction (m)*	*Tectonic movement (m)*	***Corrected altitude (m YSD)**	Data sournce
Northern Fujian	Organic silt/clay of tidal flat	27°09′32.20”	120°19′52.21”	6267 ± 776	7069	5322–8642	−1.35	−1.70 ± 1.80	0	5.80	−5.45 ± 1.80	(1)
Northern Fujian	Ostrea in living position	26°47′29.78”	120°02′58.32”	674 ± 103	202	1–411	0.70	0.30 ± 1.80	0	0.27	0.13 ± 1.80	Wang et al., 1994
Northern Fujian	Ostrea in living position	26°42′20.92”	119°34′30.56”	1394 ± 130	851	579–1151	1.00	0.30 ± 1.80	0	1.13	−0.43 ± 1.80	(2)
Northern Fujian	Organic silt/clay of tidal flat	26°39′02.85”	120°06′33.95”	1796 ± 112	1697	1414–1983	3.50	−1.70 ± 1.80	0	2.26	2.94 ± 1.80	Zeng, 1991
Northern Fujian	Organic silt/clay of tidal flat	26°36′25.31”	119°58′30.27”	891 ± 121	815	569–1058	2.00	−1.70 ± 1.80	0	1.08	2.62 ± 1.80	Zeng, 1991
Northern Fujian	Organic silt/clay of tidal flat	26°30′52.77”	119°33′53.73”	2200 ± 130	2190	1831–2690	6.25	−1.70 ± 1.80	0	2.91	5.04 ± 1.80	Lan et al., 1986
Northern Fujian	Ostrea in living position	26°26′37.90”	119°45′45.01”	1210 ± 90	677	496–894	0.50	0.30 ± 1.80	0	0.90	−0.70 ± 1.80	Xie et al., 1986
Northern Fujian	Ostrea in living position	26°20′10.27”	119°46′08.59”	833 ± 103	351	85–555	0.50	0.30 ± 1.80	0	0.47	−0.27 ± 1.80	Zeng, 1991
Northern Fujian	Shells in shell ridge	26°16′48.89”	119°41′58.64”	2100 ± 150	1589	1251–1974	6.00	4.10 ± 0.00	0	2.11	−0.21 ± 0.00	(2)
Northern Fujian	Brackish/ freshwater marsh	26°06′52.80”	119°07′48.20”	1959 ± 23	1887	1827–1975	1.60	2.10 ± 0.00	0.34	2.42	−2.58 ± 0.00	Rolett et al., 2011
Northern Fujian	Organic silt/clay of tidal flat	26°05′10.71”	119°35′58.45”	5110 ± 150	5854	5593–6186	0.00	−1.70 ± 1.80	0	4.80	−3.10 ± 1.80	Wu, 1987
Northern Fujian	Organic silt/clay of tidal flat	26°05′03.57”	119°17′50.40”	2322	2359	2059–2721	−0.02	−1.70 ± 1.80	0	3.14	−1.46 ± 1.80	Wang et al., 1990
Northern Fujian	Organic silt/clay of tidal flat	26°05′03.57”	119°17′50.40”	8000	8903	8011–9889	−16.98	−1.70 ± 1.80	0	12.29	−27.57 ± 1.80	Wang et al., 1990
Northern Fujian	Organic silt/clay of tidal flat	26°04′32.55”	119°22′46.64”	4045 ± 75	4546	4299–4824	1.26	−1.70 ± 1.80	0	3.73	−0.77 ± 1.80	Wang, 1990
Northern Fujian	Organic silt/clay of tidal flat	26°04′27.50”	119°35′25.48”	3845 ± 183	4252	3729–4821	1.28	−1.70 ± 1.80	0	3.49	−0.51 ± 1.80	(1)
Northern Fujian	Brackish/ freshwater marsh	26°03′59.50”	119°11′49.50”	8220 ± 30	9187	9027–9393	−19.50	2.10 ± 0.00	0.15	14.10	−35.55 ± 0.00	Rolett et al., 2011
Middle Fujian	Organic silt/clay of tidal flat	26°05′03.57”	119°17′50.40”	7180 ± 140	8002	7686–8334	−14.88	−1.70 ± 1.80	0	11.04	−24.22 ± 1.80	Yang, 1988
Middle Fujian	Organic silt/clay of tidal flat	25°49′06.76”	119°34′55.62”	3246 ± 160	3474	3062–3884	3.45	−1.61 ± 1.86	0	3.02	2.04 ± 1.86	(3)
Middle Fujian	Beachrock	25°38′33.04”	119°46′29.52”	3500 ± 168	3287	2836–3724	5.50	1.32 ± 1.07	0	2.86	1.32 ± 1.07	Xie et al., 1983
Middle Fujian	Beachrock	25°38′32.55”	119°46′28.73”	3015 ± 80	2700	2241–3186	4.50	1.32 ± 1.07	0	2.35	0.83 ± 1.07	Bi, 1984
Middle Fujian	Ostrea in living position	25°23′53.93”	119°06′6.49”	1420 ± 60	867	687–1052	0.50	0.26 ± 2.13	0	0.75	−0.51 ± 2.13	Zeng, 1991
Middle Fujian	Organic silt/clay of tidal flat	25°23′22.21”	119°05′20.76”	6730 ± 220	7599	7168–8007	−0.10	−1.61 ± 1.86	0	3.72	−2.21 ± 1.86	Zhang and Liu, 1993
Middle Fujian	Ostrea in living position	25°22′38.66”	119°05′44.85”	3685 ± 150	3522	3118–3936	2.40	0.26 ± 2.13	0	3.06	−0.92 ± 2.13	Zeng, 1991
Middle Fujian	Beachrock	25°13′29.49”	119°07′26.72”	3347 ± 120	3600	3173–4078	3.00	1.32 ± 1.07	0	3.13	−1.45 ± 1.07	Xie et al., 1983
Middle Fujian	Beachrock	25°12′47.49”	118°59′50.75”	4185 ± 110	4701	4417–5023	2.20	1.32 ± 1.07	0	2.30	−1.42 ± 1.07	Wu, 2002
Middle Fujian	Beachrock	25°11′48.16”	119°18′14.61”	1620 ± 70	1081	895–1276	4.00	1.32 ± 1.07	0	0.94	1.74 ± 1.07	Bi and Yuan, 1987

(*continued on next page*)

Table 1 (*continued*)

Subregion	Sediment type	Latitude	Longitude	C14 date (yr BP)	**Cal. age (cal. yr BP)**	Calibrated age (2σ, cal. yr BP)	*Altitude (m YSD)*	*Indicative meaning (m)*	*Sediment compaction (m)*	*Tectonic movement (m)*	***Corrected altitude (m YSD)**	Data sournce
Middle Fujian	Beachrock	25°11′27.89”	119°17′57.44”	2310 ± 85	1831	1574–2094	5.00	1.32 ± 1.07	0	1.59	2.09 ± 1.07	Wang, 1983
Middle Fujian	Beachrock	25°11′27.89”	119°17′57.44”	1805 ± 70	1266	1061–1469	0.00	1.32 ± 1.07	0	1.10	−2.42 ± 1.07	Bi and Yuan, 1987
Middle Fujian	Beachrock	25°09′51,75”	119°31′33.58”	3150 ± 180	2873	2398–3331	7.00	1.32 ± 1.07	0	2.50	3.18 ± 1.07	Xie et al., 1983
Middle Fujian	Beachrock	25°09′51.75”	119°31′33.58”	4000 ± 140	3920	3523–4332	6.35	1.32 ± 1.07	0	3.41	1.62 ± 1.07	Xie et al., 1983
Middle Fujian	Beachrock	25°08′28.06”	118°56′19.45”	2880 ± 85	2542	2295–2769	2.60	1.32 ± 1.07	0	2.21	−0.93 ± 1.07	Bi and Yuan, 1987
Middle Fujian	Organic silt/clay of tidal flat	24°55′29.43”	118°35′14.98”	8120 ± 160	9045	8601–9437	−10.80	−1.61 ± 1.86	0	18.54	−27.73 ± 1.86	(4)
Middle Fujian	Beachrock	24°52′19.81”	118°56′53.48”	2885 ± 139	2542	2154–2893	3.00	1.32 ± 1.07	0	2.21	−0.53 ± 1.07	Guo and Li, 1987
Middle Fujian	Organic silt/clay of tidal flat	24°32′43.43”	117°41′50.45”	4910 ± 120	5656	5327–5913	0.10	−1.61 ± 1.86	0	2.77	−1.06 ± 1.86	Chen and Huang, 1987
Middle Fujian	Mangrove	24°29′12.99”	118°05′02.41”	3459 ± 138	3728	3399–4087	1.00	2.26 ± 2.01	0	3.24	−4.50 ± 2.01	Xie, 1991
Middle Fujian	Shells in shell ridge	24°28′26.30”	117°55′58.82”	4300	4311	3713–4860	1.50	4.39 ± 0.00	0	2.11	−5.00 ± 0.00	Zheng, 1990
Middle Fujian	Shells in shell ridge	24°28′26.30”	117°55′58.82”	2350 ± 120	1882	1549–2216	2.70	4.39 ± 0.00	0	1.64	−3.33 ± 0.00	Zheng, 1990
Middle Fujian	Shells in shell ridge	24°28′26.30”	117°55′58.82”	1300	757	582–933	3.80	4.39 ± 0.00	0	0.66	−1.25 ± 0.00	Zheng, 1990
Middle Fujian	Organic silt/clay of tidal flat	24°28′17.02”	118°04′46.72”	2456 ± 145	2526	2149–2847	−3.10	−1.61 ± 1.86	0	2.20	−3.69 ± 1.86	Cai, 1988
Middle Fujian	Organic silt/clay of tidal flat	24°28′17.02”	118°04′46.72”	8960 ± 240	10,045	9493–10,679	−18.40	−1.61 ± 1.86	0	20.59	−37.38 ± 1.86	Cai, 1988
Middle Fujian	Organic silt/clay of tidal flat	24°22′41.15″	117°51′37.34”	8010 ± 40	8879	8725–9007	−8.03	−1.61 ± 1.86	0	17.17	−23.59 ± 1.86	Li, 2014
Southern Fujian	Ostrea in living position	24°28′05.85”	117°46′19.58”	3150 ± 150	2873	2462–3275	2.20	0.49 ± 1.15	0	3.28	−1.57 ± 1.15	Chen et al., 1982
Southern Fujian	Ostrea in living position	24°27′29,57”	117°45′39.18”	3330 ± 150	3083	2715–3456	2.80	0.49 ± 1.15	0	3.51	−1.20 ± 1.15	Chen et al., 1982
Southern Fujian	Organic silt/clay of tidal flat	24°26′10.88”	117°54′07.90”	602 ± 50	600	530–658	1.00	−0.78 ± 1.23	0	0.68	1.09 ± 1.23	(1)
Southern Fujian	Organic silt/clay of tidal flat	24°26′10.88”	117°54′07.90”	2051 ± 112	2009	1740–2310	−0.06	−0.78 ± 1.23	0	2.29	−1.58 ± 1.23	(1)
Southern Fujian	Organic silt/clay of tidal flat	24°26′10.88”	117°54′07.90”	7250 ± 162	8076	7752–8378	−13.78	−0.78 ± 1.23	0	11.63	−24.63 ± 1.23	(1)
Southern Fujian	Organic silt/clay of tidal flat	24°26′10.88”	117°54′07.90”	7604 ± 149	8406	8031–8760	−14.53	−0.78 ± 1.23	0	12.10	−25.86 ± 1.23	(1)
Southern Fujian	Organic silt/clay of tidal flat	24°26′10.88”	117°54′07.90”	8480 ± 157	9462	9026–9892	−20.16	−0.78 ± 1.23	0	13.63	−33.01 ± 1.23	(1)
Southern Fujian	Organic silt/clay of tidal flat	24°26′10.88”	117°54′07.90”	8779 ± 159	9845	9531–10,222	−25.86	−0.78 ± 1.23	0	14.18	−39.26 ± 1.23	(1)
Southern Fujian	Organic silt/clay of tidal flat	24°26′05.65”	117°52′58.75”	4184 ± 112	4701	4416–5029	2.00	−0.78 ± 1.23	0	3.71	−0.94 ± 1.23	(2)
Southern Fujian	Mangrove	24°26′05.65”	117°52′58.75”	4184 ± 112	4701	4416–5029	1.00	1.63 ± 1.18	0	3.71	−4.34 ± 1.18	Xie, 1991
Southern Fujian	Organic silt/clay of tidal flat	24°22′37.51”	117°51′53.89”	2180 ± 80	2176	1951–2345	2.20	−0.78 ± 1.23	0	2.48	0.49 ± 1.23	(4)
Southern Fujian	Organic silt/clay of tidal flat	24°22′37.51”	117°51′53.89”	3910 ± 90	4333	4008–4611	0.10	−0.78 ± 1.23	0	3.42	−2.55 ± 1.23	(4)

(*continued on next page*)

Table 1 (*continued*)

Subregion	Sediment type	Latitude	Longitude	C14 date (yr BP)	Cal. age (cal. yr BP)	Calibrated age (2σ, cal. yr BP)	*Altitude (m YSD)*	*Indicative meaning (m)*	*Sediment compaction (m)*	*Tectonic movement (m)*	*Corrected altitude (m YSD)	Data source
Southern Fujian	Shells in shell ridge	24°06′32.43″	117°54′22.48″	1650 ± 75	1110	910–1297	4.00	3.64 ± 0.00	0	1.27	−0.91 ± 0.00	Li, 1989
Southern Fujian	Organic silt/clay of tidal flat	24°00′08.06″	117°41′20.77″	700 ± 50	652	555–724	1.20	−0.78 ± 1.23	0	0.74	1.23 ± 1.23	Bi and Yuan, 1987
Southern Fujian	Beachrock	23°44′13.06″	117°35′29.46″	1980 ± 100	1452	1212–1716	4.00	1.05 ± 0.60	0	1.66	1.30 ± 0.06	Chen, 1986
Southern Fujian	Beachrock	23°44′13.06″	117°35′29.46″	2600 ± 120	2190	1837–2545	3.00	1.05 ± 0.60	0	2.50	−0.54 ± 0.06	Chen, 1986
Southern Fujian	Beachrock	23°44′13.06″	117°35′29.46″	3100 ± 150	2811	2391–3206	1.20	1.05 ± 0.60	0	3.20	−3.05 ± 0.06	Chen, 1986
Southern Fujian	Organic silt/clay of tidal flat	23°38′11.51″	117°24′19.67″	6640 ± 105	7519	7326–7679	5	−0.78 ± 1.23	0	5.94	−0.17 ± 1.23	Zhang et al., 1982

Notes
*Corrected altitude = Altitude − indicative meaning −sediment compaction −tectonic movement.
Data sources (1)–(4) are unpublished materials including:
(1) The Second Hydrogeological Engineering Geological Team of Fujian Province, 1986. A comprehensive investigation report on the geological and geomorphic features of the coastal zone of Fujian Province, Volume 1.
(2) The Third Institute of Oceanography, Ministry of Natural Resources of China, 1986. A comprehensive investigation report on the geological and geomorphic features of the coastal zone of Fujian Province.
(3) Xie, Z., 1985. Compilation of ^{14}C dating data for sea level change along the coast of Fujian.
(4) The Second Hydrogeological Engineering Geological Team of Fujian Province, 1990. Fujian Quaternary geological research report.

Table 2
Indicative meaning and ranges for different types of SLIPs used in this study.

Sediment type	Indicative meaning	Calculation of the indicative level	Calculation of the indicative range
Organic silt/clay of tidal flat	LLW to MTL	LLW+(MTL-LLW)/2	(MTL-LLW-MTL)/2
Shells in shell ridge	2 m above MHW	MHW + 2	0.00
Beachrock	MTL to MHW	(MTL+(MHW-MTL)/2	(MHW-MTL)/2
Ostrea in living position	MLW to MHW	MLW+(MHW-MLW)/2	(MHW-MLW)/2
Brackish/ freshwater marsh	Local MHW	MHW	0.00
Mangrove	MTL to HHW	|MTL-HHW|/2	(HHW-MTL)/2

(Table 2); (2) the SLIP should be directly dated by radiometric dating.

3.2. The calibration of the age for sea-level index points (SLIPs)

As listed in Table 1, radiocarbon ages collected in this study were determined using either the liquid scintillation counting (LSC) technique or accelerator mass spectrometry (AMS). In previous publications, some radiocarbon dates were calibrated with the international calibration curves, whereas others were not. For standardization, here we recalibrated all radiocarbon dates into calendar years before the present (BP, 1950 CE), using the Calib 8.20 software: The IntCal20 curve (Reimer et al., 2020) was used for the age calibration of terrestrial samples, while the Marine20 curve (Heaton et al., 2020) was used for the age calibration of marine samples. For samples collected in marine settings, a marine carbon reservoir effect of −66 years (δR = −66 ± 30) was used to perform the marine carbon reservoir calibration (Marine Reservoir Correction Database, http://calib.org/marine/). The carbon reservoir effect of −66 years is determined by averaging 6 reported ΔR values (recalculated from Marine20) near the Fujian coast (cf. Yoneda et al., 2007).

3.3. The correction of the elevations for sea-level index points (SLIPs)

Accurate sea-level reconstruction greatly relies on the clear definition/calibration of the indicative meaning of each SLIP. However, the reported elevation of each SLIP is influenced by both regional tectonic movements and post-depositional compaction effects (cf. Brain, 2016). Moreover, even if the SLIP's elevation is accurate enough, a precise estimate of the tidal ranges also plays an important role in calculating/modelling the past RSL position. Those above-mentioned effects were corrected according to the following procedures.

3.3.1. Tidal range correction

Many previous investigations on the Holocene RSL reconstructions assigned a uniform tidal range for the entire region. Similarly, most sea-level reconstructions for the Fujian coast used a uniform tidal range (tidal gauge observations from the Minjiangkou station) to calculate the indicative ranges for all SLIPs (e.g., Zong, 2004; Li et al., 2016). However, this may induce potential errors in sea-level reconstruction because modern tidal gauge observations have shown significant differences for different subregions of the Fujian coast (Table 3; China Gulf Chronicles Compilation Committee (CGCC), 1993). Assuming the past tidal range is similar to the modern tidal gauge observations along the Fujian coast, we here used the tidal ranges of Minjiangkou (in the northern Fujian coast), Chongwu (in the middle Fujian coast), and Dongshan (in the southern Fujian coast), to calculate the indicative meaning of SLIPs collected from the northern, middle, and southern Fujian coasts, respectively (Fig. 2c; Table 1).

Table 3
Reference tidal levels of three representative tidal gauge stations from the northern-, middle-, and southern Fujian coasts, respectively.

Subregion	Tide gauges	HHW (m)	MHW (m)	MTL (m)	MLW (m)	LLW (m)	Data source
Northern Fujian	Minjiangkou	3.7	2.1	0.1	−1.5	−3.5	Zong, 2004
Middle Fujian	Chongwu	4.26	2.39	0.25	−1.87	−3.47	1960–1983, China Gulf Chronicles Compilation Committee (CGCC), 1993
Southern Fujian	Dongshan	2.8	1.64	0.45	−0.66	−2	1960–1987, China Gulf Chronicles Compilation Committee (CGCC), 1993

Note: Tidal levels were calibrated into the National Yellow Sea Elevation datum (YSD). The averaged water levels of the three tide gauge stations are based on tidal gauge observations for the period of longer than 19 years.

3.3.2. *Correction of the sediment compaction effects and tectonic effects*

As pointed out by previous studies, sedimentary compaction can significantly change the vertical elevation of SLIPs (cf. Brain, 2016). However, due to the lack of detailed information for each SLIP, such as the borehole length, lithology, and texture composition, the effects of compaction on the vertical elevation of the SLIPs were not corrected.

The regional tectonic movements of the Fujian province are quite active and complex, especially during the Cenozoic (Li, 1988; Li, 1993; Chen et al., 2002). Considering the spatial variations in the vertical movement for different subzones (e.g., Yu and Wu, 1989; Liu et al., 1998) and taking the two NW-trending faults (Min River fault and Jiulong River fault) as natural boundaries, we here divided the Fujian Coast into three subzones (Fig. 2c), namely northern Fujian, middle Fujian, and southern Fujian, respectively. The vertical movement rate for each subzone is calculated using the following Eq. (1).

$$V = |(A - S)|/t \quad (1)$$

Where the V represents the vertical movement rate (mm/yr); A denotes the corrected elevation value of each SLIP after tidal range correction; S is the simulated past far-field eustatic sea-level position (Lambeck et al., 2014) when the SLIP is deposited/formed; and t represents the age of the SLIP. After calculation, a specific vertical movement rate of each subzone (the subregion-averaged value based on all SLIPs in the subregion) is then assigned to each SLIP collected from three different tectonic subzones, respectively.

We are aware of the fact that one of the ideal indicators of the long-term tectonic stability is the elevational difference of the previous and present interglacial marine deposits. However, to the best of our knowledge, the surface elevation of last interglacial marine deposits for the Fujian coast is not available presently. This suggests that geological data that can help address the vertical movement rates is not available for the Fujian coast. Alternatively, in many studies (e.g., Chen, 1986; Yu and Wu, 1989) the vertical tectonic movement rates were estimated as the offset between the SLIPs-based sea-level reconstructions and the global far-field sea-level variation curve, this method is also employed by this study. This is not a perfect estimation of the regional vertical tectonic movement rates since uncertainty still exists. However, as shown in Table 4, the estimated vertical movement rate (this study) is 0.82–1.38 mm/yr for the northern Fujian coast, 0.49–2.05 mm/yr for the middle Fujian coast, and 0.79–1.44 mm/yr for the southern Fujian coast, respectively. These estimations are broadly consistent with previously-reported results as listed in Table 4. Considering the consistency, we believe that our estimations of the vertical movement rates are still acceptable. Even though, additional work and datasets are needed to better constrain the regional tectonic movements, which will eventually improve the accuracy and robustness of Holocene RSL reconstructions.

3.4. *Statistics and quantitative analyses*

After all age calibrations and elevation corrections to the SLIPs were performed, an empirical Bayesian GP regression sea-level model (Khan et al., 2017; Ashe et al., 2019) was employed to generate the Holocene coastal sea-level change curve for the Fujian Coast. The generated sea-level curve integrated uncertainties in the indicative ranges and dating technique and automatically yields the estimated RLS with 1σ and 2σ uncertainties. The sea-level reconstruction was performed using the Matlab code provided by Ashe et al. (2019).

3.5. *Modelling of relative sea-level (RSL)*

To examine the GIA process and effects on Fujian sea-level change, RSL predictions were computed for this specific area using GIA models. We used three ice models: ICE-4G (Peltier, 1994), ICE-6G_C (Argus et al., 2014; Peltier et al., 2015), and a model developed at the Australian National University by Kurt Lambeck and collaborators, hereafter referred to as ANU-ICE (e.g., Lambeck and Purcell, 2005; Lambeck et al., 2014, 2017). We used the 3D Earth model HetM-LHL140 (Li and Wu, 2019) to couple with the three ice models in this study. The use of 3D Earth model is suggested by the ANU-ICE (Lambeck et al., 2014, 2017) and ICE-6G_C ice model (e.g., Li et al., 2022). The parameters of the 3D Earth model were tuned to achieve the best fit with GIA-related observational data in North America and Fennoscandia when fixed with the ICE-6G_C (e.g., Peltier et al., 2015) ice model (Li et al., 2018; Li and Wu, 2019). The GIA modelling results for the Fujian province are shown in Fig. S1.

Table 4
Range of the Holocene tectonic movement rates along Fujian coast by different studies.

Northern Fujian Coast (mm/yr)	Middle Fujian Coast (mm/yr)	Southern Fujian Coast (mm/yr)	Reference level	Time scale	Method	Data sources
−7.0 to 4.0	−7.0 to 4.0	−7.0 to 4.0	Eurasian reference frame	1972–2012	GPS observation	Wu, 2013
–	0.10–0.26	–	Eustatic sea level	Since MIS 5e	Geological reconstruction	Pedoja et al., 2008
1.81 to 2.45	1.81 to 2.45	−0.7 to 2.24	Eustatic sea level	Holocene	Geological reconstruction	Chen, 1986
0.85 to 2.68	0.9 to 1.185	0.525 to 2.8	Eustatic sea level	Holocene	Geological reconstruction	Yu and Wu, 1989
1.33 / 0.82 / 1.38	0.87 / 0.49 /2.05	1.14 / 0.79 / 1.44	Eustatic sea level	Holocene	Geological reconstruction	This study*

* Data calculated by this study: the tectonic movement rates are shown for the late Holocene (1–4 cal. kry BP), / Mid Holocene (4–8 cal. kyr BP), and / Early Holocene (8–12 cal. kyr BP), respectively. For other studies, the tectonic movement rates might only cover some of the subregions without separating different substages of the Holocene. Minus rate values denote subsidence.

4. Results

The GP regression modeled RSL changes for the Fujian coast are shown in Fig. 3. The overall Holocene sea-level variation trend for the Fujian coast generally display staged characteristics. The regional RSL rose rapidly from about −37 m to about -1 m from 10 to 7 cal. kyr BP, with an average rate of approximately 11.3 mm/a. The RSL reached its present height at about 7 cal. kyr BP and stabilized afterward. The GP regression modeled sea-level curves seems to suggest the possible existence of a mid-Holocene (from 7.5 to 5.5 cal kyr BP) sea-level highstand along the Fujian coast (Fig. 3a).

Detailed examination of the RSL curves for different subregions along the Fujian coast indicates that the general trend of Holocene sea-level variation in the northern-, middle- and southern-Fujian coast were roughly the same, but discrepancies still exist (Fig. 3). In the early Holocene (10–7 cal. kyr BP), all reconstructed regional sea-level curves for the different subzones rose rapidly, but the rate of RSL rise in the south was the highest (12.8 mm/a), followed by that for the middle Fujian (10.9 mm/a), and the northern Fujian coast (7.3 mm/a), respectively. Another significant difference among the sea-level curves of different subregions of the Fujian coast is the time when the sea-level reaches the present level: the reconstructed sea-level curves for the middle and southern Fujian coast reached near modern-day level during the mid-Holocene (ca. 7 kyr BP), but the RSL for the northern Fujian coast continued to increase until to approximately 4 cal. kyr BP. In addition, the reconstructed (mid-Holocene) sea level in the northern Fujian coast is slightly higher than modern sea level, the fluctuation in RSL is more obvious in the middle-Fujian coast than that in the northern Fujian (Fig. 3c), whereas the mid-Holocene sea level in the southern-Fujian coast is slightly lower than modern sea level (Fig. 3b, c, and d).

5. Discussion

5.1. Comparison of Holocene Sea-level reconstructions for eastern China coasts

The SLIPs-reconstructed Holocene sea-level curve for the Fujian coast is broadly consistent with previous Holocene sea-level reconstructions in China (e.g. Zong, 2004; Xiong et al., 2018, 2020; Li et al., 2021), despite this, detailed sea-level variations vary from region to region. As shown in Fig. 4, almost all reconstructed Holocene sea-level curves along the eastern China coast display three different stages: (1) the early Holocene with rapid sea-level rise; (2) the late Holocene with relatively stable sea level, and (3) the transitional middle Holocene with RSL between the above two stages. The transitional mid-Holocene is characterized by relatively high sea-level stand in several regions (e.g. Luengo et al., 2021; Zhang et al., 2021; Oliver and Terry, 2019).

Discrepancies, however, still exists: In northern China, the Holocene sea level for the western Bohai coast rose rapidly in the early Holocene but gradually stabilized at 7.5–6.8 cal. kyr BP (Fig. 4). From 6.8 to 3 cal. kyr BP, the reconstructed sea level for the western Bohai Bay coast varies by <1 m (Li et al., 2021). In the East China Sea (Xiong et al., 2020), the reconstructed sea-level (at the Hangzhou Bay) rose from −38.3 ± 1.6 m to the modern-day height during 10–7 cal. kyr BP. In the middle Holocene (7–4 cal. kyr BP), sea-level reconstruction displayed fewer variations and gradually decreased to modern-day level afterward (Fig. 4), except for a slight increase to 0.8 ± 1.4 m at 6.5 cal. kyr BP (Xiong et al.,

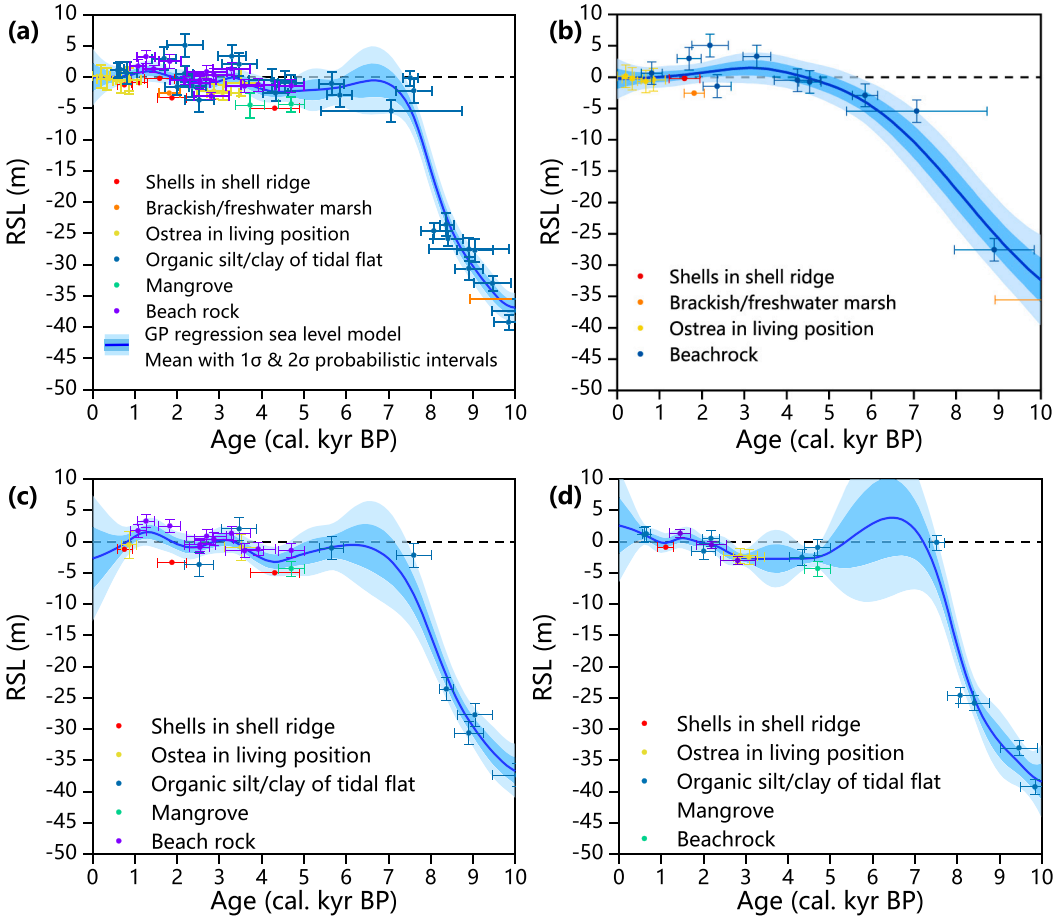

Fig. 3. SLIPs-based sea level reconstructions for the Fujian coast and subregions. (a) the entire Fujian coast database; (b) the northern Fujian coast; (c) the middle Fujian coast; (d) the southern Fujian coast.

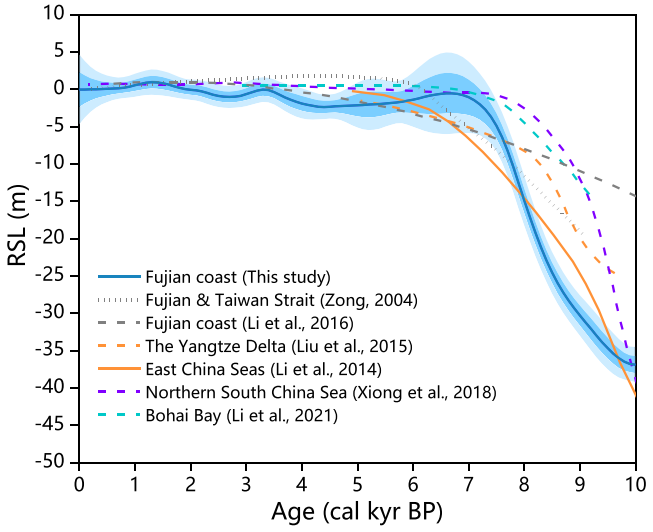

Fig. 4. Sea-level reconstructions for the Fujian coast (this study) and its comparison with other observations for different coastal regions of the China coast.

2020). In southern China, Xiong et al. (2018) revealed the Holocene RSL increased from −49.3 ± 0.8 m to the modern sea-level height during 10.5–7 cal. kyr BP (Fig. 4). However, relative sea-level variations were quite small since 7 cal. kyr (Xiong et al., 2018). In our records, Fujian coastal RSL rose rapidly from about −37 m to the modern-day height from 10 to 7 cal. kyr BP. Only minor variations in RSL were observed over the past 7 cal. kyr BP (Fig. 4).

Notable differences (Fig. 3b, c, and d) among subregional sea-level curves for the northern-, middle-, and southern-Fujian coast are also obvious, which are attributable to the special geographical location and complex tectonic background of the Fujian Province (Fig. 2). Fujian Province is located at the convergent boundary between the Pacific Ocean and Eurasia Plates (Fig. 2a). The oceanic (Philippines, Pacific) plate collided and subducted toward Taiwan Island and mainland China, resulting in continuous uplifting along the coast of Fujian. Moreover, because of the strong and active tectonic movements, NE and NW fault series (Fig. 2c) occurred frequently along the Fujian coast. Those regional-specific tectonic and crustal movement backgrounds (Chen and Liu, 2000; Zong, 2004) cast a unique regional sea-level curve for the Fujian coast that is different from other sea-level curves for the eastern China coast.

5.2. *Global meltwater discharge controls the early-Holocene Sea-level rise*

Global ice sheet dynamics have been suggested as the primary factor that dominates global sea-level change during the Pleistocene (Milne et al., 2009). Numerous geological reconstructions have confirmed that during the LGM the global mean sea level was about 120 m lower than present level because a large amount of water was frozen in the polar regions due to a significant decrease in global temperature (e.g., Mix et al., 2001). The subsequent deglaciation melted the giant glaciers and ice sheets at high latitudes and in the polar regions, causing a rise in the global mean sea-level (Mix et al., 2001; Milne et al., 2009). The ~40 m amplitude of the early-Holocene sea-level rise along the coast of Fujian was comparable to and was almost consistent with previous reconstructions in the coastal areas of eastern China and southeast Asia (Fig. 4). For example, in the Hangzhou Bay (eastern China coast) and the Pearl River Delta (southern China coast), the reconstructed sea-level variation rose rapidly from −40 m to −5 m during 10–8 cal. kyr BP (Xiong et al., 2018, 2020). In the Malay Peninsula, the SLIPs-reconstructed sea-level history also displays a rapid rise from −40 m to −5 m during the same period (Tam et al., 2018). Such similarities indicate that the early Holocene sea-level change generally follows the ice-melting equivalent sea-level (IESL) variations along the western North Pacific coasts (Xiong et al., 2020).

Despite the similarities, the patterns and rates of the early Holocene sea-level rise vary from region to region in global records. For example, in our records, the reconstructed early Holocene sea-level curve quickly increased to approximately the modern height without obvious/notable acceleration and/or plateau in the sea-level curve (Fig. 3a). Some other studies, however, have suggested that the Meltwater Pulse (MWP) may lead to an acceleration in global sea-level rise (e.g., Liu and Milliman, 2004; Bird et al., 2007; Hori and Saito, 2007). Li et al. (2014) divided the deglacial sea-level variation into seven stages, including four accelerated-rising stages and three slowdown-rising stages, among which the accelerated-rising stages were suggested to be linked to MWP events (Li et al., 2014). In the reconstructed Western Pacific sea-level curve (Liu et al., 2004), three rapid sea-level rise stages were recognized and have been attributed to three MWP events since the last 12 kyr BP. Bird et al. (2007) also recognized an acceleration in the early Holocene sea-level in Singapore (approximately at 7.3 kyr BP) which is slightly later than the MWP-2 event (7.6–7.5 cal. kyr BP, cf. Blanchon et al., 2002), after a relatively stable sea-level stage during 8–7.3 cal. kyr BP.

However, those MWP-like events were not apparent in our SLIPs-based sea-level reconstructions (Fig. 3). One reason might be that the complex local tectonic movements have overlay the MWP-like sea-level rise. Another possible reason is the paucity of SLIPs used to generate the Holocene sea-level curves. As shown in Fig. S2, there are only 12 SLIPs spanning the period from 10 cal. kyr BP to 7 cal. kyr BP. The lack of SLIPs prevents a thorough understanding of early Holocene sea-level curve for the Fujian coast. Despite the above-mentioned deficiency, our SLIPs still have captured the general trend of sea-level history along the Fujian coast. This study demonstrates that the early-Holocene sea-level change was primarily influenced by global meltwater discharge.

5.3. *The possibility of mid-Holocene Sea-level highstand*

The possible existence of a mid-Holocene sea-level highstand represents one of the most controversial and debatable issues in Quaternary sea-level change studies. The mid-Holocene climate optimum, also called mid-Holocene thermal maximum, is a well-known warm period that opens a possibility for the sea-level highstand (cf. Guilcher, 1969). Globally, many sites provide evidence of higher than present sea level dated back to the mid- to late-Holocene, such as in Argentina (Luengo et al., 2021), Malay Peninsula (Zhang et al., 2021), Thailand (Oliver and Terry, 2019), and Australia (Dougherty et al., 2019), etc. According to the times and heights of the mid-Holocene sea-level highstand recorded from tectonically stable sites in the tropics, Zong (2013) proposed that the amplitude of mid-Holocene sea-level highstand decreases from its maximum at the equator toward mid-latitudes or intermediate-field sites where highstand are not recorded. In terms of the timing of the sea-level highstand in the tropics, variations exist among different sites: records from the southeastern coast of India showed that the sea-level highstand started at around 7430 to 7190 cal. yr BP, whereas records from the Central New South Wales of Australia showed the highstand occurred at 5500–4800, and 3600–1500 cal. yr BP (Zong, 2013). Along the south coast of China, a mid-Holocene sea-level highstand of approximately 1 m above the present-day sea-level has been reported (Zong, 2004).

Some other studies, however, argued that the Holocene sea-level highstand assumption is explainable by either GIA or regional crustal movement effects (e.g., Zong, 2004, 2013). Among them, GIA effects represent the dynamic response of solid Earth to mass redistribution of ice/water during a glacial-interglacial cycle (Peltier, 1999). The effects of GIA are more significant in the near-field areas than that in the far-field regions (Peltier, 1999). For East Asia, which is located in the mid-latitudes, the effects of GIA on regional sea-level change have seldomly been investigated or discussed. However, there are two main processes that can modulate sea-level variation in the far-field region

and thus should be taken into consideration in explaining the far-field regional sea-level reconstructions (Mitrovica and Milne, 2002): (1) Ocean syphoning effects, which refers to the redistribution of water from far-field oceanic basins to the site of collapsing peripheral bulges, resulting in RSL fall in far-field oceanic basins; (2) Continental levering effects, which refers to a tilting of the continental margins due to the increased ocean-loading following deglaciation, leading to a decrease in RSL both in the near- and far-fields (Mitrovica and Milne, 2002).

There has been an improvement in the ability of numerical models to predict the spatial and temporal patterns of RSL changes for the eastern China coast (e.g., Bradley et al., 2016 and reference therein). In our reconstruction, the GP model estimated a possible highstand of Fujian coastal sea level from 7.1 to 5.9 cal. kyr BP (within 2σ uncertainties). The upper limit of the 1σ uncertainty can be as high as 2.5 m, which is comparable to the height and timing of the previously reported mid-Holocene sea-level highstand on the South China Sea coast (Fig. 3; Zong, 2004; Xiong et al., 2018). Our reconstructions broadly agree with the China region-specific model of Holocene ice-volume equivalent sea-level change (Fig. 5; Bradley et al., 2016), which is characterized as an initial slowdown in the rate of RSL rise at 7 cal. kyr BP, associated with the final deglaciation of the Laurentide ice sheet (cf. Bradley et al., 2016). In the ICE-6G_C, the projected Fujian coastal sea level rose rapidly until 8 cal. kyr BP, when there was a marked slowdown in the rate of melting. Following a secondary minor slowdown at 7 cal. kyr BP, the ICE-6G_C model suggests the RSL reached to a stabilized level about 1 millennium earlier than in our SLIPs-based reconstruction (Fig. 5). The ANU-ICE RSL modelling differs from the ICE-6G_C RSL modelling in the timing of the initial slowdown in RSL rise (7 kyr BP versus 8 kyr BP) and the amplitude of Holocene sea-level highstand: the ANU-ICE RSL predictions displayed an initial slowdown in the rate of RSL rise at 7 kyr BP with lowered (than ICE-6G_C predictions) highstand levels during the mid- and late-Holocene.

Misfits between the model predictions and SLIPs based sea-level reconstructions are also obvious: (1) our RSL reconstructions were significantly lower than the China-specific RSL model and ICE-6G_C model predictions during the early-Holocene; (2) both our SLIPs-based reconstructions and China-specific RSL model didn't show significant highstand whereas the ICE-6G_C model and ANU-ICE model suggest a mid-Holocene sea-level highstand of about 3 m, and 1.5 m for the Fujian coast, respectively (Fig. 5); (3) Since the mid- to late-Holocene (7 cal. kyr BP to present), our reconstructed sea-level fluctuated around the modern-day sea-level (similar to the China-specific RSL model predictions, Bradley et al., 2016) but the ICE-6G_C model and ANU-ICE model predicted RSLs gradually decreased to modern levels due to the 'ocean syphoning' and 'continental levering' effects (Mitrovica and Milne, 2002).

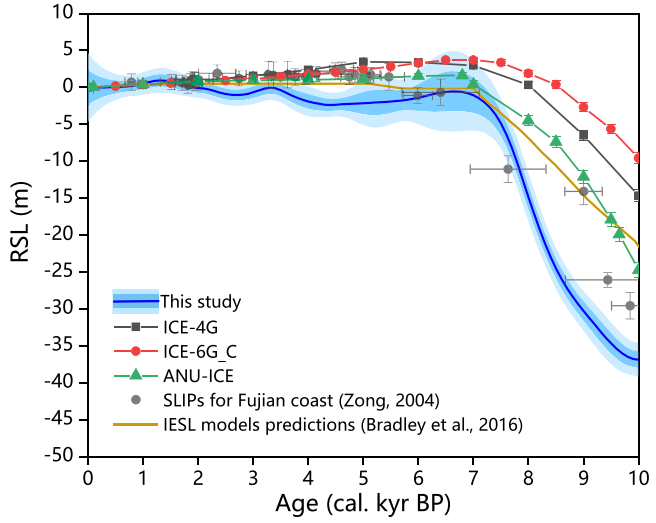

Fig. 5. Comparison of SLIPs-reconstructed Fujian coastal sea-level (this study) with the relative sea-level predictions from ice-volume equivalent sea level (Bradley et al., 2016), and GIA models with ICE-4G, ICE-6G_C, and ANU-ICE.

Chua et al. (2021) also reported a mismatch between the SLIPs-based estimation and GIA-process-based predictions in the Singapore (far-field) coastal sea-level reconstructions: mid-Holocene sea-level highstand occurred at ca. 7 cal. kyr BP in the GIA modeled predictions but occurred at around 5 cal. kyr BP in the SLIPs-estimated reconstructions. Chua et al. (2021) attributed the data-model difference to local-specific tectonic movements (such as subsidence of continental shelf) and/or uncertainties in the time and amount of the ice-sheet melting when predicting the past sea-level positions. As both Fujian and Singapore are located in far-field regions, the reasons for the misfits between our SLIPs-estimated sea level and GIA-process-based predictions are similar. Xiong et al. (2020) compared sea-level datasets from the Malay Peninsula and Hangzhou Bay (the eastern China coast) and have concluded that the GIA effects for the Cathaysia-Yangtze blocks (southeastern China) and the Sundaland are different, possibly due to differences in geological settings and differences in the upper mantle viscosity between these two landmasses (Bradley et al., 2016; Xiong et al., 2020): Fujian province is located within the Eurasian Plate and is surrounded by active subduction zones (e.g. Liu et al., 2022). Along the southeastern coast of China, the Pacific and Philippine sub-plate subducts below the Eurasian plate (Fig. 2) whereas the Malay-Thailand Peninsula sits within a geologically stable region called Sundaland. Despite the relatively close geographical distance and similar general tectonic setting, the shallow earth structure below China appears to be more geodynamically complex than that below Malay-Thailand. Bradley et al. (2016) used data-model comparisons to suggest that the obvious mid-Holocene sea-level highstand as predicted in GIA-process models is attributable to the stronger mantle viscosity parameter used in the VM2 earth model. Such parameter coupling with the ICE-5G model generated a significant highstand at 8 kyr BP for the China sites (Bradley et al., 2016). When lower mantle viscosity values were used, the amplitude of the mid-Holocene highstand significantly decreased (cf. Bradley et al., 2016 and reference therein).

Our records and China-specific IESL modelling suggest no significant highstand along the Fujian coast (Fig. 5; Bradley et al., 2016), however, it is still unwise to reject the possibility of mid-Holocene sea-level highstand due to the fact that there are sparse SLIPs spanning the mid-Holocene (from 7 cal. kyr BP to 4 cal. kyr BP). The temporal distribution of our Holocene SLIPs is uneven, with >74% points after 5 cal. kyr BP (Fig. S2). The database lacks SLIPs between 8 and 5 cal. kyr BP (<5%), resulting in a less-robust estimation of the amplitude and variation characteristics of mid-Holocene sea-level change. Additional Holocene SLIPs along the Fujian coast are needed before a robust conclusion can be reached.

Moreover, a previous examination of the spatial pattern of predicted sea level along the coastline of China (using the ICE-5G VM2 GIA model) shows that there is no notable difference between the northern and central China coast, implying that the observed diverse spatial variability in China coastal sea-level curves is not due to GIA but to other processes. Therefore, an improved understanding and/or better estimation of the localized factors, such as coastal geometries, and tectonic movements might be needed for the understanding of the "mid-Holocene highstand" hypothesis (cf. Zong, 2004, 2013).

5.4. *Late-Holocene relative sea-level (RSL) variations*

The late-Holocene RSL records of the Fujian coast are relatively well constrained (Fig. S2). Unlike the GIA model predictions, the reconstructed sea level fluctuated significantly over the last 4 millennia despite a generally increasing trend to the present level. Particularly, SLIPs-based curve indicates two RSL lowstands during the intervals at ~4.4 cal. kyr BP and ~ 2.4 cal. kyr BP, and a highstand of ~1 m during

1.8 to ~0.7 cal. kyr. BP. The timing of the sea-level lowstands chronologically corresponds to the 4.2 kyr BP and 2.8 cal. kyr BP ice-rafted debris (IRD) events as recorded in the North Atlantic (Bond et al., 1997, 2001), whereas the ~1 m sea-level highstand might correspond to the Medieval Warm Period, suggesting a potential climate-cooling (warming) induced sea-level fall (rise). Kench et al. (2020) present evidence for two low sea-level phases in the Indian Ocean and concluded that RSL lowstands are coincident with cooler periods during the Late Antique Little Ice Age (~1500 to 1300 cal. yr BP) and the Little Ice Age (~700 to 100 cal. yr BP). Meltzner et al. (2017) also reported about ~0.6 m fluctuations in the mid-Holocene RSL history in which the lowstands of RSL might be linked to climatic cooling in the tropical Pacific Ocean. There is increasing evidence suggesting that oscillations may be more common than previously appreciated, particularly in the mid- to late-Holocene, during which no major ice sheet melting was observed since 6 kyr BP (Bradley et al., 2016).

Both the ICE-6G_C model and ANU-ICE model predict a near-linear RSL fall during the late-Holocene without going below modern sea-level, despite a difference in the predicted height (Fig. 5). Similarly, Lambeck et al. (2014) also found no evidence of fluctuations in far-field sea-level reconstructions for the late-Holocene, indicating that regional climate fluctuations are not likely to induce significant global sea-level oscillations. Moreover, using principles of sea-level physics, Piecuch et al. (2021) challenged the hypothesis of climate-driven sea-level lowstand (Meltzner et al., 2017; Kench et al., 2020) and concluded that pre-industrial radiative forcing and sea surface temperature (SST) changes were insufficient to cause thermosteric sea-level trends as large as reported in Kench et al. (2020).

Explanations for the reconstructed oscillations in the late-Holocene sea-level curves for the Fujian coast can be attributed to: (1) localized tectonic movements due to the geological history of the study region. Any incorrect/improper estimate of the uplift or subsidence rates of crustal movements can cause a significant bias in RSL, resulting in a highstand or a lowstand of the SLIPs-based sea-level reconstruction. (2) Uncertainties in past sea-level reconstruction. Sediment compaction, erosion, and post-depositional process could change the elevation of each SLIP significantly. Due to a lack in proper parameters, the compaction, and erosion rates could not be accurately estimated, which may cause a significant bias in the elevation estimate of each SLIP and caused apparent oscillation in the sea-level curves. Future studies are needed to decipher the possible local explanations for Late-Holocene sea-level oscillations.

6. Conclusive remarks

In this paper, we re-evaluated the published data and produced a standardized Holocene RSL database of 59 SLIPs for the Fujian coast. This allowed us to compare data from different far-field regions to obtain insights into the processes driving Holocene RSL changes in far-field regions. The reconstructed RSL rose rapidly from −37 m to about −1 m during 10–7 cal. kyr BP, with a rate of approximately 11.3 mm/yr. The mean values of estimated RSL didn't show an obvious mid-Holocene highstand except for the interval of 7.5–5.5 cal. kyr BP during which the 2σ upper limit of the estimated RSL is above present sea level. The nature of the mid-Holocene highstand, however, remains poorly understood because of the paucity of SLIPs. The late-Holocene RSL for the Fujian coast is characterized as a series of fluctuations that may correspond to global/regional warming or cooling events, such as IRD events or Medieval Warm Period. The reasons for the late-Holocene RSL fluctuation remain controversial and can be attributed to either climate variations or localized crustal movements.

We further compared the RSL reconstructions for the Fujian coast with the latest iteration of GIA models to better understand the driving mechanisms of temporal and spatial variability in Holocene RSL. We show there are substantial misfits between GIA predictions and regional RSL reconstructions: (1) the termination of the rapid sea-level rise was about 1000 years earlier in the ICE-6G_C model than in the SLIPs-based reconstructions; (2) GIA model predictions show a mid-Holocene sea-level highstand of 1–3 m which is absent in our SLIPs-based reconstructions; and (3) all GIA models predicted a gradual RSL fall to 0 m without an RSL lowstand below present, while our reconstruction displays significant RSL oscillations. It is unknown whether these misfits are caused by regional processes, such as possible crustal movements or inaccurate parameters used in the GIA model.

The findings from this study contribute toward an improved knowledge of the Holocene sea-level behavior in far-field regions. However, future standardized Holocene RSL data and further constraints on the GIA models will aid in better understanding the driving mechanisms of Holocene RSL variations along the Fujian coastal region.

Declaration of Competing Interest

The authors declare that they have no known competing financial interests or personal relationships that could have appeared to influence the work reported in this paper.

Data availability

All data supporting the main findings of this study are included in the text as tables.

Acknowledgments

This work was financially supported by the National Natural Science Foundation of China (Grant No. 42076207 to Fengling Yu); the Fundamental Research Funds for the Central Universities of Xiamen University (Grant No. 20720190096 to Fengling Yu); the China Postdoctoral Science Foundation (Grant No. 2021M691862 to Nannan Li); the Singapore Ministry of Education Academic Research Fund MOE2019-T3-1-004 and MOE-T2EP50120-0007, the National Research Foundation Singapore, and the Singapore Ministry of Education, under the Research Centers of Excellence initiative (to Tanghua Li). Prof. Steven A. Kuehl is acknowledged for kindly reading and commenting on an early version of the manuscript and language corrections. We thank W. Richard Peltier for providing the ICE-4G and ICE-6G_C ice model and Kurt Lambeck and Anthony Purcell for providing the ANU-ICE ice model. The global ANU-ICE combination model used in this study was kindly provided by Holger Steffen. The GIA modelling is conducted in part using the research computing facilities and/or advisory services offered by Information Technology Services, the University of Hong Kong. This work is Earth Observatory of Singapore contribution 523.

Appendix A. Supplementary data

Supplementary data to this article can be found online at https://doi.org/10.1016/j.palaeo.2023.111577.

References

Argus, D.F., Peltier, W.R., Drummond, R., Moore, A.W., 2014. The Antarctica component of postglacial rebound model ICE-6G_C (VM5a) based on GPS positioning, exposure age dating of ice thicknesses, and relative sea level histories. Geophys. J. Int. 198 (1), 537–563.

Ashe, E.L., Cahill, N., Hay, C., Khan, N.S., Kemp, A., Engelhart, S.E., Horton, B.P., Parnell, A.C., Kopp, R.E., 2019. Statistical modeling of rates and trends in Holocene relative sea level. Quat. Sci. Rev. 204, 58–77.

Bassett, S.E., Milne, G.A., Mitrovica, J.X., Clark, P.U., 2005. Ice sheet and solid earth influences on far-field sea-level histories. Science 309, 925–928.

Bi, F., 1984. Basic features of Neotectonic movement in the middle Fujian coast. J. Earth Sci. Environ. 1, 27–33 (in Chinese).

Bi, F., Yuan, Y., 1987. A preliminary Study on Coastal rise and fall periods in the Coast of Fujian and Guangdong in the past 5000 years. Sci. Sin. Chim. 4, 429–440 (in Chinese).

Bird, M.I., Austin, W.E.N., Wurster, C.M., Fifield, L.K., Mojtahid, M., Sargeant, C., 2010. Punctuated eustatic sea-level rise in the early mid-Holocene. Geology 38, 803–806.

Bird, M.I., Fifield, L.K., Teh, T.S., Chang, C.H., Shirlaw, N., Lambeck, K., 2007. An inflection in the rate of early mid-Holocene eustatic sea-level rise: a new sea-level curve from Singapore. Estuar. Coast. Shelf Sci. 71, 523–536.
Blanchon, P., Jones, B., Ford, D.C., 2002. Discovery of a submerged relic reef and shoreline off Grand Cayman: further support for an early Holocene jump in sea level. Sediment. Geol. 147, 253–270.
Bond, G., Showers, W.J., Cheseby, M., Lotti, R., Almasi, P., Demenocal, P., Priore, P., Cullen, H., Hajdas, I., Bonani, G., 1997. A pervasive millennial-scale cycle in North Atlantic Holocene and glacial climates. Science 278 (5341), 1257–1266.
Bond, G., Kromer, B., Beer, J., Muscheler, R., Evans, M.N., Showers, W., Hoffman, S., Lotti-Bond, R., Hajdas, I., Bonani, G., 2001. Persistent Solar Influence on North Atlantic climate during the Holocene. Science 294, 2130–2136.
Bradley, S.L., Milne, G.A., Horton, B.P., Zong, Y., 2016. Modelling Sea level data from China and Malay-Thailand to estimate Holocene ice-volume equivalent sea level change. Quat. Sci. Rev. 137, 54–68.
Brain, M.J., 2016. Past, present and future perspectives of sediment compaction as a driver of relative sea level and coastal change. Curr. Clim. Change Rep. 2, 75–85.
Cai, L., 1988. A preliminary study on ZK3702 Quaternary micropaleobiocoensis and marine transgression of Xiamen Yuandang Harbour, Fujian. Geol. Fujian 7, 178–185 +253-257 (in Chinese with English abstract).
Carlson, A.E., Clark, P.U., 2012. Ice sheet sources of sea level rise and freshwater discharge during the last deglaciation. Rev. Geophys. 50, RG4007.
Chen, C., Huang, B., Wang, M., 1982. Studies of Holocene Geochronology in the coastal regions of Southern Fujian. Taiwan Strait 2, 64–73 (in Chinese).
Chen, F., 1986. The formation of beach rock in the Gulei Peninsula and the sea level changes in the coastal region of the Southern Fujian.. In: China Sea Level Changes. China Ocean Press, Beijing, pp. 166–172 (in Chinese).
Chen, W.S., Yang, H.C., Wang, X., Huang, H., 2002. Tectonic setting and exhumation history of the Pingtan-Dongshan Metamorphic Belt along the coastal area, Fujian Province, Southeast China. J. Asian Earth Sci. 20, 829–840.
Chen, Y., Huang, Y., 1987. Discussion on Neotectonic movement in Zhangzhou Basin, Fujian Province. South China Seismol. J. 1, 1–15 (in Chinese).
Chen, Y.G., Liu, T.K., 2000. Holocene uplift and subsidence along an active tectonic margin southwestern Taiwan. Quat. Sci. Rev. 19, 923–930.
China Gulf Chronicles Compilation Committee (CGCC), 1993. China Gulf Chronicle (Volume 7): Gulfs in Southern Fujian Province. China Ocean Press, Beijing (in Chinese).
Chua, S., Switzer, A.D., Li, T., Chen, H., Christie, M., Shaw, T.A., Khan, N.S., Bird, M.I., Horton, B.P., 2021. A new Holocene Sea-level record for Singapore. The Holocene 31, 1376–1390.
Clark, P.U., Mix, A.C., 2002. Ice sheets and sea level of the last Glacial Maximum. Quat. Sci. Rev. 21, 1–7.
Costas, S., Ferreira, Ó., Plomaritis, T.A., Leorri, E., 2016. Coastal barrier stratigraphy for Holocene high-resolution sea-level reconstruction. Sci. Rep. 6, 38726.
Cuzzone, J.K., Clark, P.U., Carlson, A.E., Ullman, D.J., Rinterknecht, V.R., Milne, G.A., Lunkka, J.P., Wohlfarth, B., Marcott, S.A., Caffee, M., 2016. Final deglaciation of the Scandinavian Ice Sheet and implications for the Holocene global sea-level budget. Earth Planet. Sci. Lett. 448, 34–41.
Dougherty, A.J., Thomas, Z.A., Fogwill, C., Hogg, A., Palmer, J., Rainsley, E., Williams, A.N., Ulm, S., Rogers, K., Jones, B.G., Turney, C., 2019. Redating the earliest evidence of the mid-Holocene relative sea-level highstand in Australia and implications for global sea-level rise. PLoS ONE 14 (7), e0218430.
Engelhart, S.E., Horton, B.P., 2012. Holocene Sea level database for the Atlantic coast of the United States. Quat. Sci. Rev. 54, 12–25.
Fang, G., Li, P., Huang, G., 1992. Holocene Sea level changes in southern Fujian and Eastern Guangdong. Quat. Sci. 3, 233–240 (in Chinese with English abstract).
Fox-Kemper, B., Hewitt, H.T., Xiao, C., Aðalgeirsdóttir, G., Drijfhout, S.S., Edwards, T.L., Golledge, N.R., Hemer, M., Kopp, R.E., Krinner, G., Mix, A., Notz, D., Nowicki, S., Nurhati, I.S., Ruiz, L., Sallée, J.-B., Slangen, A.B.A., Yu, Y., 2021. In: Masson-Delmotte, V., Zhai, P., Pirani, A., Connors, S.L., Péan, C., Berger, S., Caud, N., Chen, Y., Goldfarb, L., Gomis, M.I., Huang, M., Leitzell, K., Lonnoy, E., Matthews, J. B.R., Maycock, T.K., Waterfield, T., Yelekçi, O., Yu, R., Zhou, B. (Eds.), Ocean, Cryosphere and Sea Level Change. In Climate Change 2021: The Physical Science Basis. Contribution of Working Group I to the Sixth Assessment Report of the Intergovernmental Panel on Climate Change. Cambridge University Press, Cambridge, United Kingdom and New York, NY, USA, pp. 1211–1362. https://doi.org/10.1017/9781009157896.011.
García-Artola, A., Stéphan, P., Cearreta, A., Kopp, R.E., Khan, N.S., Horton, B.P., 2018. Holocene Sea-level database from the Atlantic coast of Europe. Quat. Sci. Rev. 196, 177–192.
Gehrels, W.R., Shennan, I., 2015. Sea level in time and space: revolutions and inconvenient truths. J. Quat. Sci. 30, 131–143.
Guilcher, A., 1969. Pleistocene and Holocene Sea level changes. Earth Sci. Rev. 5, 69–97.
Guo, X., 1979. Sea level changes since late Pleistocene in China. Sci. Geol. Sin. 4, 330–341 (in Chinese with English abstract).
Guo, Y., Li, Q., 1987. Evolution of Meizhou Bay, Fujian Province. J. Trop. Oceanogr. 2, 19–27 (in Chinese with English abstract).
Heaton, T.J., Köhler, P., Butzin, M., Bard, E., Reimer, R.W., Austin, W.E.N., Ramsey, C.B., Grootes, P.M., Hughen, K.A., Kromer, B., 2020. Marine20—the marine radiocarbon age calibration curve (0–55,000 cal BP). Radiocarbon 62 (4), 779–820.
Hijma, M.P., Engelhart, S.E., Törnqvist, T.E., Horton, B.P., Hu, P., Hill, D.F., 2015. A protocol for a geological sea-level database. In: Handbook of Sea-Level Research. John Wiley & Sons Ltd, pp. 536–553.
Hori, K., Saito, Y., 2007. An early Holocene Sea-level jump and delta initiation. Geophys. Res. Lett. 34, L18401.
Horton, B.P., Gibbard, P.L., Mine, G.M., Morley, R.J., Purintavaragul, C., Stargardt, J.M., 2005. Holocene Sea levels and palaeoenvironments, Malay-Thai Peninsula, Southeast Asia. The Holocene 15, 1199–1213.
Kench, P.S., Owen, S.D., Beetham, E.P., Mann, T., McLean, R.F., Ashton, A., 2020. Holocene Sea level dynamics drive formation of a large atoll island in the Central Indian Ocean. Glob. Planet. Chang. 195, 103354.
Khan, N.S., Ashe, E., Horton, B.P., Dutton, A., Kopp, R.E., Brocard, G., Engelhart, S.E., Hill, D.F., Peltier, W.R., Vane, C.H., Scatena, F.N., 2017. Drivers of Holocene sea-level change in the Caribbean. Quat. Sci. Rev. 155, 13–36.
Khan, N.S., Ashe, E., Shaw, T.A., Vacchi, M., Walker, J., Peltier, W.R., Kopp, R.E., Horton, B.P., 2015. Holocene relative sea-level changes from near-, intermediate-, and far-field locations. Curr. Clim. Change Rep. 1, 247–262.
Khan, N.S., Horton, B.P., Engelhart, S., Rovere, A., Vacchi, M., Ashe, E.L., Törnqvist, T.E., Dutton, A., Hijma, M.P., Shennan, I., 2019. Inception of a global atlas of sea levels since the last Glacial Maximum. Quat. Sci. Rev. 220, 359–371.
Kopp, R.E., Horton, B.P., Kemp, A.C., Tebaldi, C., 2015. Past and future sea-level rise along the coast of North Carolina, USA. Clim. Chang. 132, 693–707.
Lambeck, K., Esat, T., Potter, E.K., 2002. Links between climate and sea levels for the past three million years. Nature 419, 199–206.
Lambeck, K., Purcell, A., 2005. Sea-level change in the Mediterranean Sea since the LGM: model predictions for tectonically stable areas. Quat. Sci. Rev. 24, 1969–1988.
Lambeck, K., Purcell, A., Zhao, S., 2017. The north American late Wisconsin ice sheet and mantle viscosity from glacial rebound analyses. Quat. Sci. Rev. 158, 172–210.
Lambeck, K., Rouby, H., Purcell, A., Sun, Y., Sambridge, M., 2014. Sea level and global ice volumes from the Last Glacial Maximum to the Holocene. Proc. Natl. Acad. Sci. 111, 15296–15303.
Lan, D., Yu, Y., Chen, C., Xie, Z., 1986. Preliminary study on late Pleistocene transgression and Holocene Sea-level fluctuation in Fuzhou Basin. Mar. Geol. Quat. Geol. 6 (3), 103–111 (in Chinese with English abstract).
Li, G., Li, P., Liu, Y., Qiao, L., Ma, Y., Xu, J., Yang, Z., 2014. Sedimentary system response to the global sea level change in the East China Seas since the last glacial maximum. Earth Sci. Rev. 139, 390–405.
Li, J., 1993. Tectonic framework and evolution of southeastern China. J. SE Asian Earth Sci. 8, 219–223.
Li, J., Shang, Z., Wang, F., Chen, Y., Tian, L., Jiang, X., Yu, Q., Wang, H., 2021. Holocene Sea level trend on the west coast of Bohai Bay, China: reanalysis and standardization. Acta Oceanol. Sin. 40, 198–248.
Li, P., 1989. A Chronological Study of the Sandy Embankments along the South China Coast. Chin. Sci. Bull. 12, 928–931 (in Chinese with English abstract).
Li, T., Khan, N.S., Baranskaya, A.V., Shaw, T.A., Peltier, W.R., Stuhne, G.R., Wu, P., Horton, B.P., 2022. Influence of 3D Earth Structure on Glacial Isostatic Adjustment in the Russian Arctic. J. Geophys. Res. Solid Earth 127, e2021JB023631.
Li, T., Wu, P., 2019. Laterally heterogeneous lithosphere, asthenosphere and sub-lithospheric properties under Laurentia and Fennoscandia from Glacial Isostatic Adjustment. Geophys. J. Int. 216 (3), 1633–1647.
Li, T., Wu, P., Steffen, H., Wang, H., 2018. In search of laterally heterogeneous viscosity models of glacial isostatic adjustment with the ICE-6G_C global ice history model. Geophys. J. Int. 214 (2), 1191–1205.
Li, Y., 2014. Stratigraphy and the sedimentary environments in Fujian coast since the Late Quaternary. Chin. Acad. Sci. 1–186. PhD thesis.
Li, Y., Xu, L., Xu, B., 2016. Changes of sea-level in Fujian coast during the past 40000 years. J. Neijiang Norm. Univ. 31 (6), 46–55 (in Chinese with English abstract).
Li, Z., 1988. A preliminary study of formation mechanism of tectonic landform of Fujian. J. Fujian Teachers Univ. (Nat. Sci.) 4 (2), 94–99 (in Chinese with English abstract).
Liu, J.P., Milliman, J.D., 2004. Reconsidering melt-water pulses 1A and 1B: global impacts of rapid sea-level rise. J. Ocean Univ. China 3, 183–190.
Liu, J.P., Milliman, J.D., Gao, S., Cheng, P., 2004. Holocene development of the Yellow River's subaqueous delta, North Yellow Sea. Mar. Geol. 209, 45–67.
Liu, P., Zhang, J., Wang, J., Lin, F., Lin, Y., Yu, J., Liu, Y., Zhang, D., Sun, Q., Sun, D., Chen, J., Chen, Z., 2022. Tectonic subsidence of the Southeast China coast: New evidence from late Pleistocene transgression in Ningde bay. Palaeogeogr. Palaeoclimatol. Palaeoecol. 605, 111226.
Liu, Y., Guo, F., Chen, Z., Huang, L., Ma, Q., 1998. Recent crustal vertical movement and fault activity of Fujian Province. Crustal Deform. Earthq. 18 (4), 68–73 (in Chinese with English abstract).
Liu, Y., Sun, Q., Fan, D., Dai, B., Ma, F., Xu, L., Chen, J., Chen, Z., 2018. Early to Middle Holocene Sea level fluctuation, coastal progradation and the Neolithic occupation in the Yaojiang Valley of southern Hangzhou Bay, Eastern China. Quat. Sci. Rev. 189, 91–104.
Liu, Y., Sun, Q., Thomas, I., Zhang, L., Finlayson, B., Zhang, W., Chen, J., Chen, Z., 2015. Middle Holocene coastal environment and the rise of the Liangzhu City complex on the Yangtze delta, China. Quat. Res. 84 (3), 326–334.
Luengo, M.S., Ballesteros-Prada, A., Vilanova, I., Bernasconi, E., Fucks, E., 2021. Environmental changes related to the Holocene Sea-level transgression and successive highstand (7–5.5 Kyr) at the NE coastal plain of Buenos Aires (Argentina). Quat. Int. 602, 4–14.
Mauz, B., Vacchi, M., Green, A., Hoffmann, G., Cooper, A., 2015. Beachrock: a tool for reconstructing relative sea level in the far-field. Mar. Geol. 362, 1–16.
Meltzner, A.J., Switzer, A.D., Horton, B.P., Ashe, E., Qiu, Q., Hill, D.F., Bradley, S.L., Kopp, R.E., Hill, E.M., Majewski, J.M., Natawidjaja, D.H., Suwargadi, B.W., 2017. Half-metre Sea-level fluctuations on centennial timescales from mid-Holocene corals of Southeast Asia. Nat. Commun. 8, 14387.
Milne, G.A., Gehrels, W.R., Hughes, C.W., Tamisiea, M.E., 2009. Identifying the causes of sea-level change. Nat. Geosci. 2, 471–478.
Mitrovica, J.X., Milne, G.A., 2002. On the origin of late Holocene Sea-level highstands within equatorial ocean basins. Quat. Sci. Rev. 21, 2179–2190.

Mix, A.C., Bard, E., Schneider, R., 2001. Environmental processes of the ice age: land, oceans, glaciers (EPILOG). Quat. Sci. Rev. 20, 627–657.
Oliver, G.J.H., Terry, J.P., 2019. Relative Sea-level highstands in Thailand since the Mid-Holocene based on 14C rock oyster chronology. Palaeogeogr. Palaeoclimatol. Palaeoecol. 517, 30–38.
Pedoja, K., Shen, J.W., Kershaw, S., Tang, C., 2008. Coastal Quaternary morphologies on the northern coast of the South China Sea, China, and their implications for current tectonic models: a review and preliminary study. Mar. Geol. 255 (3/4), 103–117.
Peltier, W.R., 1994. Ice age paleotopography. Science 265, 195–201.
Peltier, W.R., 1999. Global sea level rise and glacial isostatic adjustment. Glob. Planet. Chang. 20, 93–123.
Peltier, W.R., 2004. Global glacial isostasy and the surface of the ice-age earth: the ICE-5G (VM2) model and GRACE. Annu. Rev. Earth Planet. Sci. 32, 111–149.
Peltier, W.R., Argus, D.F., Drummond, R., 2015. Space geodesy constrains ice age terminal deglaciation: the global ICE-6G_C (VM5a) model. J. Geophys. Res. Solid Earth 120, 450–487.
Peltier, W.R., Wu, P.P.C., Argus, D., Li, T., Velay-Vitow, J., 2022. Glacial isostatic adjustment: physical models and observational constraints. Rep. Prog. Phys. 85, 096801.
Piecuch, C.G., Kemp, A.C., Gebbie, G., Meltzner, A.J., 2021. Climate did not drive Common Era Maldivian Sea-level lowstands. Nat. Geosci. 14, 273–275.
Reimer, P.J., Austin, W.E.N., Bard, E., Bayliss, A., Blackwell, P.G., Ramsey, C.B., Butzin, M., Cheng, H., Edwards, R.L., Friedrich, M., 2020. The IntCal20 Northern Hemisphere radiocarbon age calibration curve (0–55 cal kBP). Radiocarbon 62 (4), 725–757.
Rolett, B.V., Zheng, Z., Yue, Y., 2011. Holocene Sea-level change and the emergence of Neolithic seafaring in the Fuzhou Basin (Fujian, China). Quat. Sci. Rev. 30 (7–8), 788–797.
Shi, X., Liu, S., Yang, S., Liu, Q., Tan, J., Guo, Z., 2015. Spatial–temporal distribution of storm surge damage in the coastal areas of China. Nat. Hazards 79, 237–247.
Slangen, A.B., Church, J.A., Agosta, C., Fettweis, X., Marzeion, B., Richter, K., 2016. Anthropogenic forcing dominates global mean sea-level rise since 1970. Nat. Clim. Chang. 6, 701–705.
Stanford, J.D., Hemingway, R., Rohling, E.J., Challenor, P.G., Medina-Elizalde, M., Lester, A.J., 2011. Sea-level probability for the last deglaciation: a statistical analysis of far-field records. Glob. Planet. Chang. 79, 193–203.
Tam, C.Y., Zong, Y., Bin Hassan, K., Bin Ismal, H., Binti Jamil, H., Xiong, H., Wu, P., Sun, Y., Huang, G., Zheng, Z., 2018. A below-the-present late Holocene relative sea level and the glacial isostatic adjustment during the Holocene in the Malay Peninsula. Quat. Sci. Rev. 201, 206–222.
Wang, F., Li, J., Chen, Y., Fang, J., Zong, Y., Shang, Z., Wang, H., 2015. The record of mid-Holocene maximum landward marine transgression in the west coast of Bohai Bay, China. Mar. Geol. 359, 89–95 (in Chinese).
Wang, F., Wang, H., Li, J., Wang, F., Tian, L., Yu, Q., Huang, Z., Fang, J., Hu, Y., Xiao, G., Li, C., 2023. Evolution and trending prediction of the chinese mainland coasts since 20 ka BP: Implication for ecological protection and restoration. Geol. China 50 (1), 61–83 (in Chinese with English abstract).
Wang, F., Zong, Y., Mauz, B., Li, J., Fang, J., Tian, L., Chen, Y., Shang, Z., Jiang, X., Spada, G., Melini, D., 2020. Holocene Sea-level change on the central coast of Bohai Bay, China. Earth Surf. Dyn. 8, 679–693.
Wang, L., Wang, Z., Li, C., 2022. Holocene relative sea-level change of Fujian coast, southeastern China: Geological records and comparison with glacio-hydro isostatic adjustment modelling. Haiyang Xuebao 44 (9), 109–123 (in Chinese with English abstract).
Wang, S., Wu, X., 1992. Climate and sea level changes during Holocene high temperature period along Fujian coast. J. Oceanogr. Taiwan Strait 11 (4), 345–352 (in Chinese with English abstract).
Wang, S., Yang, J., Sun, H., Zeng, C., Yu, M., Wu, X., 1990. Post-glacial Sea level movement in the lower reaches of the Minjiang River and adjacent areas. Acta Oceanol. Sin. 12 (1), 64–74 (in Chinese).
Wang, S., Yang, J., Zeng, C., Wu, X., Yu, M., 1994. Sea level changes since late Pleistocene along Fujian coast. J. Oceanogr. Taiwan Strait 13 (2), 166–175 (in Chinese with English abstract).
Wang, Y., 1990. The classification of Quaternary strata in Fujian Province. Geol. Fujian 4, 289–306.
Wang, Z., Zhan, Q., Long, H., Saito, Y., Gao, X., Wu, X., Li, L., Zhao, Y., 2013. Early to mid-Holocene rapid sea-level rise and coastal response on the southern Yangtze delta plain, China. J. Quat. Sci. 28, 659–672.
Wang, Z., Zhuang, C., Saito, Y., Chen, J., Zhan, Q., Wang, X., 2012. Early mid-Holocene Sea-level change and coastal environmental response on the southern Yangtze delta plain, China: implications for the rise of Neolithic culture. Quat. Sci. Rev. 35, 51–62.
Woodroffe, S.A., Horton, B.P., 2005. Holocene Sea-level changes in the Indo-Pacific. J. Asian Earth Sci. 25, 29–43.
Wu, X., 1987. On the causes of the peat formation along the coast of Fujian Province. Trop. Geogr. 7 (3), 219–227 (in Chinese with English abstract).
Wu, X., 2002. Rates of the vertical movements of the fault blocks along the coast of Fujian Province during the last 10000 years. J. Minjiang Univ. 2, 41–46 (in Chinese).
Wu, X.L., 2013. Crustal Deformation Characteristics Analysis and Three-dimensional Velocity Inversion of Changle-Nan'ao Faults. Master thesis of Chang'an University, Xi'an, China, 63p. (in Chinese).
Xie, Z., 1991. Proceeding of the symposium on geology and seismology in the Taiwan Strait region. In: Ocean Press, Beijing, pp. 163–169 (in Chinese).
Xie, Z., Chen, F., Liu, W., Shao, H., Xu, Z., 1983. Fujian Holocene beachrock and the sealevel changes. Taiwan Strait 2 (1), 61–70+126-127 (in Chinese).
Xie, Z., Shao, H., Chen, F., Chen, Z., Dou, Y., 1986. Late Pleistocene marine transgression along the Fujian coast. In: China Sea Level Changes. China Ocean Press, pp. 156–165 (in Chinese).
Xiong, H., Zong, Y., Li, T., Long, T., Huang, G., Fu, S., 2020. Coastal GIA processes revealed by the early to middle Holocene Sea-level history of East China. Quat. Sci. Rev. 233, 106249.
Xiong, H., Zong, Y., Qian, P., Huang, G., Fu, S., 2018. Holocene Sea-level history of the northern coast of South China Sea. Quat. Sci. Rev. 194, 12–26.
Yang, J., 1988. Estimates of sedimentary compaction in sea level studies. J. Appl. Oceanogr. 4, 382–388 (in Chinese with English abstract).
Yang, J., Zheng, X., 1990. Sea-level fluctuations during the past 6000 years along the coast of Fujian. Mar. Geol. Quat. Geol. 10 (4), 67–75 (in Chinese with English abstract).
Yoneda, M., Uno, H., Shibata, Y., Suzuki, R., Kumamoto, Y., Yoshida, K., Sasaki, T., Suzuki, A., Kawahata, H., 2007. Radiocarbon marine reservoir ages in the western Pacific estimated by pre-bomb molluscan shells. Nucl. Inst. Methods Phys. Res. B 259, 432–437.
Yu, Z., Wu, X., 1989. Rates of Holocene vertical movements of fault blocks along the coast of Fujian Province. Seismol. Geol. 11 (3), 27–33 (in Chinese with English abstract).
Zeng, C., 1991. Sea level variation along Fujian coast in Holocene. J. Oceanogr. Taiwan Strait 10 (1), 77–84 (in Chinese with English abstract).
Zhang, D., Liu, W., 1993. Relation between coast-change and climate over past 4000a BP in Putian, Fujian. J. Appl. Oceanogr. 1, 85–89.
Zhang, J., Li, G., Zhao, X., 1982. Chronological studies on the late quaternary stratigraphy and Neotectonic movement along the coastal area of South Fujian and East Guangdong. Seismol. Geol. 3, 27–36+83 (in Chinese).
Zhang, Y., Zong, Y., Xiong, H., Li, T., Fu, S., Huang, G., Zheng, Z., 2021. The middle-to-late Holocene relative sea-level history, highstand and levering effect on the east coast of Malay Peninsula. Glob. Planet. Chang. 196, 103369.
Zheng, X., 1990. The overlapping chanier in the North bank of Jiulongjiang estuary and the sea level changes in the late Holocene. Mar. Sci. 3, 17–21 (in Chinese).
Zheng, Y.F., Xiao, W.J., Zhao, G., 2013. Introduction to tectonics of China. Gondwana Res. 23, 1189–1206.
Zong, Y., 2004. Mid-Holocene Sea-level highstand along the Southeast Coast of China. Quat. Int. 117, 55–67.
Zong, Y., 2013. Late Quaternary relative sea-level changes in the tropics. In: Elias, S.A. (Ed.), Encyclopedia of Quaternary Science (Second Edition). Elsevier, pp. 495–502.